

Role of Core Support Material in Veneer Failure of Brittle Layer Structures

Ilja Hermann, Sanjit Bhowmick, Brian R. Lawn

Materials Science and Engineering Laboratory, National Institute of Standards and Technology, Gaithersburg, Maryland 20899-8500

Received 30 June 2006; revised 8 August 2006; accepted 22 August 2006
Published online 31 October 2006 in Wiley InterScience (www.interscience.wiley.com). DOI: 10.1002/jbm.b.30712

Abstract: A study is made of veneer failure by cracking in all-ceramic crown-like layer structures. Model trilayers consisting of a 1 mm thick external glass layer (veneer) joined to a 0.5 mm thick inner stiff and hard ceramic support layer (core) by epoxy bonding or by fusion are fabricated for testing. The resulting bilayers are then glued to a thick compliant polycarbonate slab to simulate a dentin base. The specimens are subjected to cyclic contact (occlusal) loading with spherical indenters in an aqueous environment. Video cameras are used to record the fracture evolution in the transparent glass layer *in situ* during testing. The dominant failure mode is cone cracking in the glass veneer by traditional outer (Hertzian) cone cracks at higher contact loads and by inner (hydraulically pumped) cone cracks at lower loads. Failure is deemed to occur when one of these cracks reaches the veneer/core interface. The advantages and disadvantages of the alumina and zirconia core materials are discussed in terms of mechanical properties—strength and toughness, as well as stiffness. Consideration is also given to the roles of interface strength and residual thermal expansion mismatch stresses in relation to the different joining methods. © 2006 Wiley Periodicals, Inc. *J Biomed Mater Res Part B: Appl Biomater 82B: 115–121, 2007

Keywords: cone cracks; alumina; zirconia; dental crowns; cyclic fatigue; slow crack growth; residual stress

INTRODUCTION

Brittle materials loaded at their top surfaces with curved indenters are subject to cone-shaped fractures initiating from prepresent flaws within the Hertzian contact field.^{1,2} In single-cycle loading, outer cone fractures form immediately beyond the expanding contact and flare outward and downward at a shallow angle to the specimen surface. In multi-cycle loading, in aqueous environments, additional, inner cone fractures form well within the maximum contact and penetrate more steeply and deeply.^{3,4} The latter variety of cone crack is dangerous because its downward growth is strongly enhanced by hydraulic pumping of liquid into the crack interfaces.⁵ In brittle layer structures consisting of one functional ceramic (veneer) bonded onto a second, stiff and strong structural ceramic support (core), with the composite veneer/core structure subsequently joined to a compliant base, cone cracks can quickly penetrate to the veneer/core interface and cause failure, even at low loads.⁶ Such trilayer configurations are particularly relevant to occlusal contact of all-ceramic crowns on dentin.⁷ Cone cracking is not the only

mode of potential failure: median cracks can initiate from quasiplastic zones immediately below the contact⁸; radial cracks can initiate from flaws at the core undersurface.⁹ Median cracks can be suppressed by maintaining a sufficiently large cuspal radius, radial cracks by maintaining a sufficiently large net veneer/core thickness. Given that such suppressant conditions can be met, failure of the structure reduces to a competition between outer and inner cone cracks within the veneer layer.

In forming real crown-like structures, it is necessary to join the veneer to the core. This is generally done by fusion at elevated temperatures to form a strong adherent bond. However, fusion can introduce significant residual stresses in both layers unless great care is taken to match the coefficients of thermal expansion (CTE).^{6,10} Such residual stresses can be substantial unless the CTE mismatch is extremely small, and, because they superpose onto the Hertzian and flexural stresses from the contact field, will enhance or inhibit crack growth toward the interface (depending on whether they are tensile or compressive). These stresses are not easy to avoid. A potential alternative approach is to join the two layers at lower temperatures, e.g. by physical bonding with a strong polymer-based adhesive. This approach runs the risk of producing softer and weaker interfaces, leading to yet other potential fracture modes including delamination at the interface and radial cracking at the bottom of the flexing veneer.¹¹

Correspondence to: B. R. Lawn (e-mail: Brian.lawn@nist.gov)
Contract grant sponsor: National Institute of Dental and Craniofacial Research;
Contract grant number: PO1 DE10976.

© 2006 Wiley Periodicals, Inc. *This article is a US Government work and, as such, is in the public domain in the United States of America.

Given the necessary restrictions on choice of porcelain veneer layer imposed by the requirements of aesthetics, questions then arise as to the best core support material to minimize veneer cone cracking, as well as any other mode of failure. Intuitively, the core should be stiff to provide support for the veneer, and strong, to avoid failure of the core itself. Questions also arise as to the related role of CTE mismatch stresses. To answer these questions we conduct cyclic Hertzian contact tests on model flat layer structures consisting of a glass plate (representing porcelain veneer) joined either by fusion or epoxy bonding to alumina or zirconia (Y-TZP) plates (representing most common core ceramics).⁶ Tests are conducted using tungsten carbide sphere indenters in a water environment. The transparency of glass enables direct viewing of the veneer cone crack failure modes. Data on numbers of cycles to achieve a failure state are determined as a function of peak contact load for specimens for each core ceramic and for each joining mode. The relative merits of the two ceramic materials in relation to prevention of veneer cracking are considered.

EXPERIMENTAL

Layer Specimen Fabrication

A model trilayer system similar to that used previously was adopted.⁶ Essential properties of the materials used are listed in Table I. For the upper (veneer) layer, soda-lime glass microscope slides (Fischer Scientific, Pittsburgh, PA) of thickness 1 mm were cut into plates 25 mm². The top surfaces of the plates were abraded with SiC grit to provide starting flaws for the ensuing cone cracks. The edge faces were polished for direct side viewing during testing. For the support (core) layer, plates of alumina (AD995, CoorsTek, Golden, CO) and Y-TZP zirconia (Lava Frame, 3M ESPE, Morrow, GA) 0.5 mm thick and 12.5 mm² in area were diamond-polished to 1 μm finish, to avert spurious core failures. These materials may be considered representative of those used in all-ceramic dental crowns, the glass with similar modulus and toughness to veneering porcelain and the alumina and zirconia with similar properties to core ceramics.

The soda-lime glass and core ceramic plates were then bonded together to form bilayers of net thickness 1.5 mm. One group was adhesively-bonded with epoxy resin (Harcos Chemicals, Bellesville, NJ). The epoxy interface was kept thin (< 20 μm) to minimize flexure of the outer layer during subsequent contact testing.¹¹ This bonding method produced specimens without significant residual fabrication stresses. A second group was fusion-bonded using adhesive glass tape

TABLE I. Parameters for Materials in This Study

Material	E (GPa)	Poisson's Ratio	CTE (10^{-6} K^{-1})
Glass	70	0.22	10.3
Y-TZP	205	0.22	11.0
Al_2O_3	370	0.22	8.0

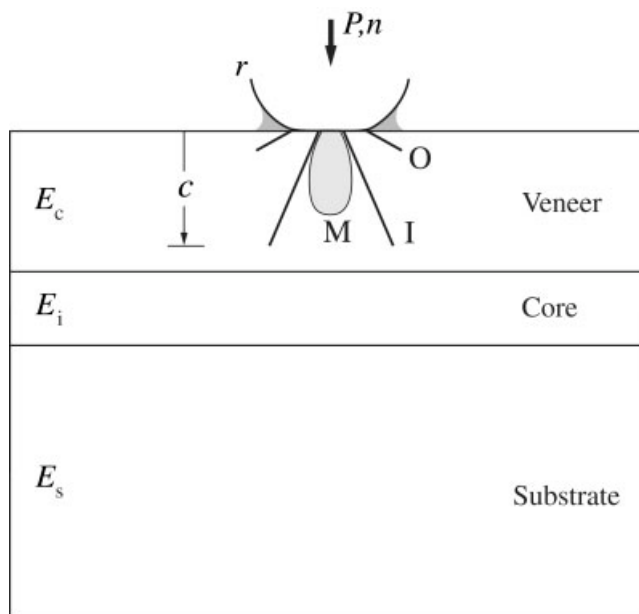


Figure 1. Schematic of crack geometry for cyclic contact on brittle veneer/core layer bonded to compliant support base with sphere of radius r at load P for number of cycles n in water (shaded). Showing top-surface veneer crack modes of characteristic through-thickness depth c : outer cone cracks (O), inner cone cracks (I), and median cracks (M). Inner and median cracks are sometimes hard to distinguish in glass, so any M data are collectively lumped in with I data in subsequent figures. Additional radial cracks can occur at veneer or core bottom surfaces and delamination cracks at veneer/core interface (not shown).

(G-1001 transfer tape, Vitta Corp, Bethel, CT) heated to 600°C. This tape has similar modulus and CTE to soda-lime glass, but differs from that of the ceramic core (Table I). The interfacial glass layer had a thickness $\approx 50 \mu\text{m}$. The cooled bilayer specimens showed some signs of curvature, indicating the presence of residual flexural stresses.⁶

Some all-glass specimens were prepared as controls to investigate any effects of the different interlayers on lifetimes. Glass/glass bilayers were formed by joining 1 mm and 0.5 mm plates using the same epoxy and glass-tape bonding described above. Monolithic 1.5 mm thick soda-lime glass slides were used as effective glass/glass bilayers with a virtual interface of infinitesimal thickness at 1 mm depth. As before, the top surfaces of these specimens were pre-abraded and the side surfaces polished.

The specimens thus prepared were then adhesively bonded at their bottom surfaces onto a compliant polycarbonate slab 12.5 mm thick (Hyzod, AIN Plastics, Norfolk, VA) using epoxy resin to produce the final configuration in Figure 1. The polycarbonate base simulates the compliant dentin support in natural tooth structure.

Fracture Testing

Contact testing and *in situ* side viewing of the crack evolution were carried out as indicated in Figure 1.¹² A WC indenter of radius $r = 1.58 \text{ mm}$ was mounted into the crosshead of a fatigue testing machine (Model 5500R, Instron Corp, Canton,

MA) and loaded onto the specimen top surfaces.^{3,4,6} Periodic loads were imposed up to $n = 10^6$ cycles at a frequency of 1 Hz, with maximum value ranging from $P_m = 700$ N down to $P_m = 70$ N and minimum value 2 N (the latter to prevent indenter wandering). All tests were conducted in water, replenished drop by drop at the contact site, providing access to the cone cracks throughout the experiment.

A video camera was set up for side viewing through the polished glass sides. Cone crack depths c were recorded at the deepest points of penetration as a function of number of cycles n (Figure 1). Failure was deemed to occur when the deepest crack intersected the bonded glass/core interface or, in the case of the glass monoliths, crossed a virtual interface, at depth $c = 1$ mm below the top surface. In most cases, glass failure occurred from an outer or inner cone, depending on P_m . Occasionally, failures occurred from median cracks, but these were often difficult to distinguish from inner cone cracks and were thus lumped in with inner cone data.⁶ No other modes of primary failure were observed in the current experiments, although some secondary delamination was observed in epoxy-bonded specimens.

Stress Analysis

A commercially available analytical computational algorithm for computing elastic fields in layer structures subject to indentation (FilmDoctor v 0.996b, Saxonian Institute for Surface Mechanics, Eilenburg, Germany; available at <http://www.esae.de/products>) was used to evaluate Hertzian stresses in the glass/ceramic double layers.^{6,13} A separate finite element algorithm was used to evaluate superposed residual CTE mismatch stresses, as described in a preceding article.⁶ Independently determined input parameters for these calculations are included in Table I. Principal stresses acting normal to the contact axis were determined at specified loads for each glass/core layer system. While these stresses are not those acting directly on the inclined cone crack surfaces, they nevertheless provide insight into the forces that act to drive or inhibit crack extension through the thickness of the glass veneer layer.

RESULTS AND ANALYSIS

Experimental Data

The first set of results in Figure 2 are for tests on control glass/glass specimens of net thickness 1.5 mm formed by different joining methods: (a) virtual interface (monolith plate), (b) epoxy-bonded interface, and (c) fused interface. The points are $c(n)$ data for a peak cyclic load $P_m = 300$ N. Individual tests are distinguished by different symbols. The horizontal dashed line at $c = 1$ mm corresponds to failure of the veneer; the vertical dashed line indicates the critical number of cycles n_F to reach this state. Outer cone cracks (O) form first and grow steadily with number of cycles. Inner cone cracks (I) form later but quickly overtake their predecessors and lead to failure. There is no discernible shift in data between specimen types in Figure 2, with an apparently com-

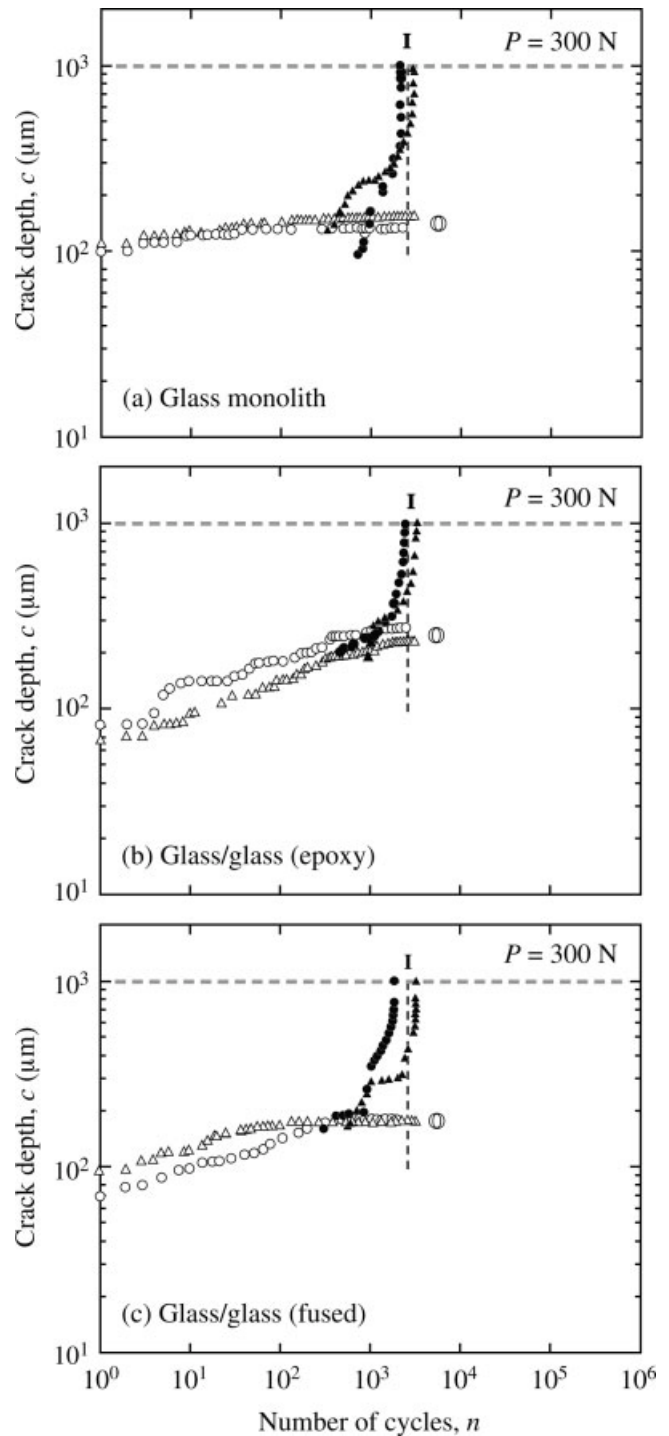


Figure 2. Crack depth c as function of number of cycles n at frequency 1 Hz for 1 mm/0.5 mm glass/glass bilayers glued to polycarbonate base, with different interfaces: (a) virtual (monolith glass); (b) epoxy-bonded; (c) glass-tape-fused. Data for indentation with WC sphere of radius $r = 1.58$ mm at fixed peak load $P_m = 300$ N, tests in water. Different symbols indicate separate tests. Outer cone cracks (O) initiate first but inner cone cracks (I) propagate to failure after critical number of cycles n_F (vertical dashed line) when crack penetrates veneer layer to interface (horizontal dashed line).

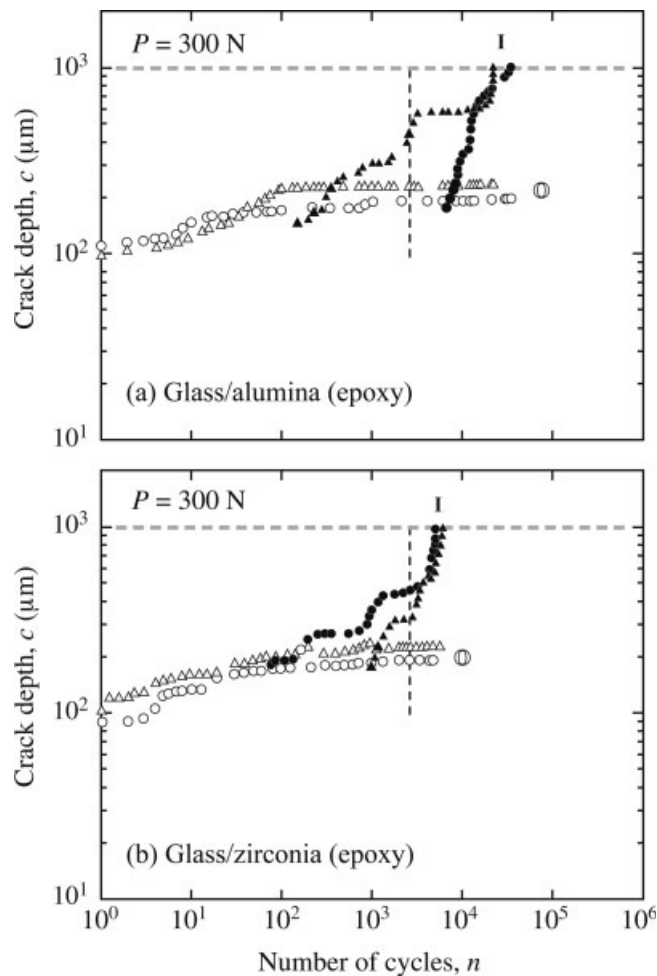


Figure 3. Crack depth c as function of number of cycles n at frequency 1 Hz in water for epoxy-bonded glass/ceramic bilayers on polycarbonate base: (a) glass/alumina and (b) glass/zirconia. Data for indentation with WC sphere of radius $r = 1.58$ mm at fixed peak load $P_m = 300$ N, two tests per indenter.

mon failure lifetime $n_F = 2-3 \times 10^3$ cycles. This commonality confirms that any residual stresses from the joining method are sufficiently small that they have no demonstrable effect on the cone crack evolution.

Further observation of the crack growth revealed some differences in behavior once the I cracks reached the interface. For the monolith [Figure 2(a)] and fused specimens [Figure 2(c)], the cracks continued their accelerating growth beyond 1 mm into the sublayer, requiring only a few additional cycles to penetrate the entire specimen. For the epoxy-bonded specimens [Figure 2(b)], the same I cones arrested at the interface and required a substantial increase in the cycling to cause full failure by delamination. These differences in behavior reflect the strengths of the respective interfaces.

The next set of results was obtained on epoxy-bonded glass/core specimens. Figure 3 shows $c(n)$ data for (a) glass/alumina and (b) glass/zirconia specimens, again at $P_m = 300$ N. The failure evolution is similar to that in Figure 2, i.e. O cones initiating first but failures ultimately occurring from

I cones. The vertical dashed line at $n_F = 2-3 \times 10^3$ cycles is carried over from the glass/glass data in Figure 2, for comparison. Thus, specimens with alumina cores show more than an order of magnitude longer lifetime relative to all-glass specimens, whereas specimens with zirconia cores show a smaller positive shift. Delamination of the interface was observed to occur somewhat later in the testing, at a number of cycles well in excess of n_F . These results indicate that a stiffer core does provide some beneficial support for the veneer, at least in specimens without significant residual stresses.

The results in Figure 3 relate to one peak contact load, $P_m = 300$ N. Tests at different loads P_m for specimens with the same epoxy-bonded interfaces reveal strong variations in the critical number of cycles n_F , and even a change in failure mode.⁶ $n_F(P_m)$ data are plotted in Figure 4 for glass/glass, glass/alumina, and glass/zirconia specimens. Points represent individual failures, lines are empirical fits to the glass/glass data only (to establish a baseline for comparison). O cones initiate first at all loads. At high loads, in the region $P_m = 400-600$ N, failure occurs exclusively from the same O cones, before I cones can initiate. In this region, n_F is sensitive to P_m , but not so much to core material, at least within the scatter of data. At low loads, $P_m < 400$ N, failure occurs from later-developing I cones. In this region n_F is much less sensitive to P_m , and failures can occur down to $P_m < 100$ N, highlighting the danger posed by I cracks in prolonged cyclic loading. However, the data for different cores now diverge markedly, with alumina providing the longest lifetimes followed by zirconia and then glass, again in accordance with expectation from core stiffness.

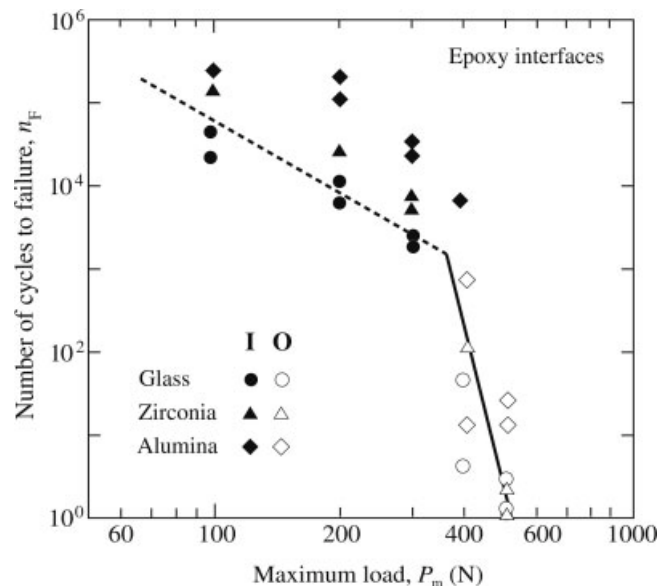


Figure 4. Number of cycles to failure n_F as function of maximum contact load P_m for epoxy-bonded glass/ceramic bilayers on polycarbonate base. Cyclic indentation with WC spheres of radius $r = 1.58$ mm, frequency 1 Hz, in water. Failure occurs from O cones (unfilled symbols) at higher loads, from I cones (filled symbols) at lower loads. Lines are empirical fits to glass/glass data. Some alumina data courtesy Juan José Meléndez-Martínez.

A third set of tests was made on fused glass/core specimens. In this instance, no strong attempt was made to match CTE stresses between the soda-lime glass and alumina or zirconia ceramic core, other than to ensure that the mismatch was small enough that the specimens did not delaminate spontaneously during fabrication. Figure 5 shows $c(n)$ data for (a) glass/alumina and (b) glass/zirconia at $P_m = 300$ N (cf. Figure 2). The data shifts for the alumina and zirconia cores relative to all-glass specimens (vertical dashed line at $n_F = 2-3 \times 10^3$ cycles) are now reversed, i.e., it is the zirconia that has the longer lifetimes, the alumina the lower. These results indicate that the stiffness of the core itself is not the sole factor governing lifetime, but that the nature of the interfacial fusion between dissimilar materials must also play a role.

Figure 6 shows $n_F(P_m)$ data for glass/glass, glass/alumina, and glass/zirconia specimens with fused interfaces (cf. Figure 3). Again, points represent individual failures, lines are empirical fits to the glass/glass data only. As in Figure 5, zirconia

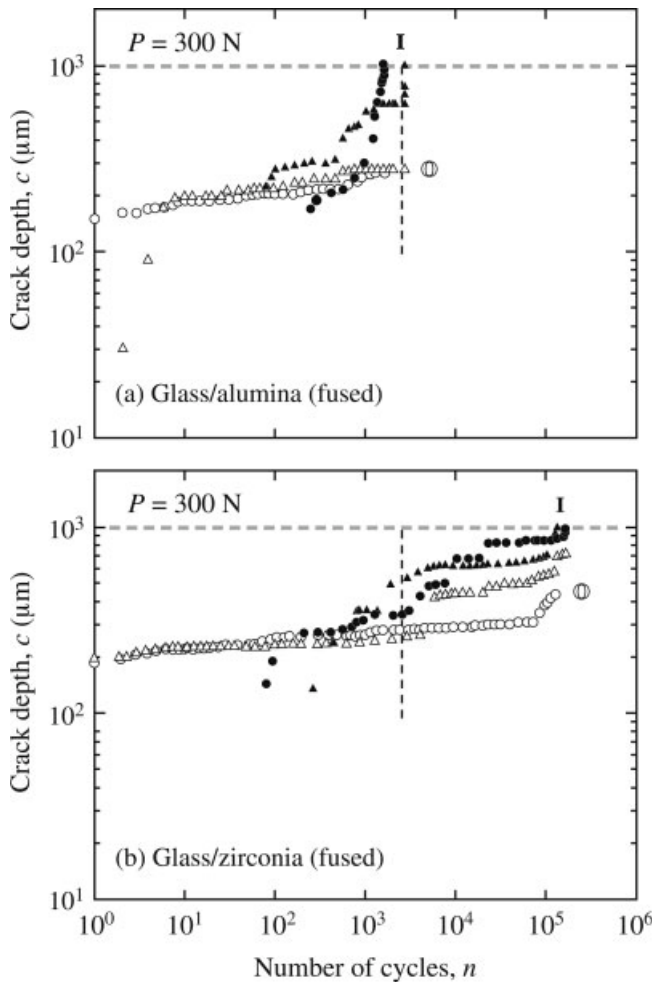


Figure 5. Crack depth c as function of number of cycles n at frequency 1 Hz in water for glass-tape-fused glass/ceramic bilayers on polycarbonate base: (a) glass/alumina and (b) glass/zirconia. Data for indentation with WC sphere of radius $r = 1.58$ mm at fixed peak load $P_m = 300$ N, two tests per indenter.

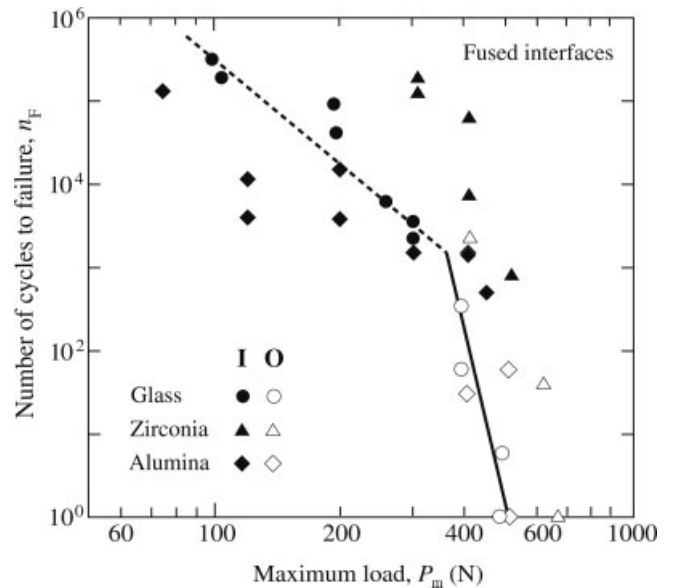


Figure 6. Number of cycles to failure n_F as function of maximum contact load P_m for glass-tape-fused glass/ceramic bilayers on polycarbonate base. Cyclic indentation with WC spheres of radius $r = 1.58$ mm, frequency 1 Hz, in water. Failure occurs from O cones at higher loads, from I cones at lower loads. Lines are empirical fits to glass/glass data. Some alumina data courtesy Juan José Meléndez-Martínez.

shows the longest lifetimes, alumina the lowest, the latter falling even below all-glass in the low-load region. We shall argue below that this reversal is due to the superposition of residual CTE stresses onto the contact loading field.

Analysis

Figure 7 plots radial stress normal to the contact axis as a function of distance from the glass/ceramic interface for alumina and zirconia, and glass core layers from contact with WC spheres of radius $r = 1.58$ mm at load $P = 300$ N. We are concerned primarily with stresses in the top glass layer, where the O and I cracks form, but the stresses are also plotted in the ceramic core layer for completeness. (The presence of a 20 μ m epoxy interlayer has only minor effect on these stresses, so we neglect this interlayer in the present calculations.) Note how stresses in the veneer layer for specimens with zirconia and (especially) alumina cores revert to compression on approaching the interface. These trends are attributable to an increasing constraint on the adjacent veneer from the more rigid cores.¹⁴ They also account for the relative data shifts to higher lifetimes for alumina and (to a lesser extent) zirconia in Figures 3 and 4.

To explain the data shifts in Figures 5 and 6, it is necessary to take into account CTE mismatch between the glass and ceramic core layers. Computed radial stress distributions through the glass/core thicknesses are shown in Figure 8.⁶ The most pertinent feature of these stresses is a buildup of tension within the glass layer near the interface with the alumina core, and a corresponding buildup of compressive stresses

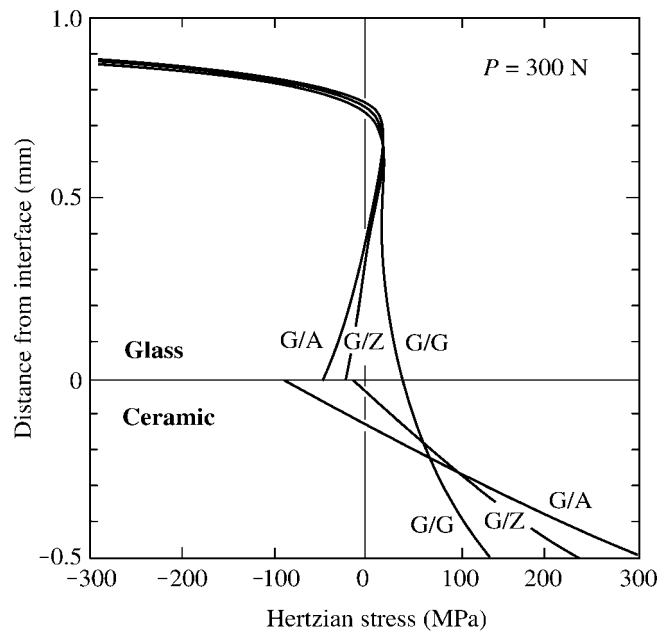


Figure 7. Distribution of radial stresses along contact axis in contact/flexure field in glass/alumina (G/A) and glass/zirconia (G/Z) bilayers relative to all-glass control (G/G), for bilayer with ideal interface and polycarbonate base. Indentation with WC spheres of radius $r = 1.58$ mm at load $P = 300$ N.

near the interface with the zirconia core. These stresses, superposed onto those from the contact loading in Figure 7, explain the reversed data shifts in Figures 3 and 5. Note that the CTE stresses, because they are independent of P , may be expected to dominate at lower contact loads, i.e. in the region where the data for different cores diverge most markedly in Figures 4 and 6.

DISCUSSION

This study has examined the role of a stiff core support material in the failure of brittle coatings in glass/ceramic layer structures, simulating veneer failure in all-ceramic dental crowns. In fabricating model structures for evaluation of failure modes, we have chosen soda-lime glass for the outer layer and alumina or zirconia (Y-TZP) for the core layer. These materials have essentially similar mechanical properties (elastic modulus, strength, and toughness) to dental porcelains (glass) and ceramic cores (alumina and zirconia). The veneer/core bilayers have been glued to a polycarbonate slab to simulate a compliant dentin base. The transparency of the glass enables direct viewing of cone fracture in contact loading within the veneer from initiation to failure. Two bonding methods have been used to join the veneer and core layers: epoxy adhesive and glass-tape fusion. The results on epoxy-bonded specimens show that a stiffer core, especially alumina, can indeed be beneficial as an inhibitor of cone crack failure in the veneer by suppressing tensile stresses close to the interface.¹⁴ However, comparative results on fused specimens suggest that such benefits can be severely

compromised by residual stresses from veneer/core CTE mismatch. In our experiments, the alumina has a lower CTE than the glass, resulting in deleterious tensile stresses in the veneer close to the interface, overwhelming any benefits of modulus mismatch. The effect is opposite in specimens with zirconia cores, which show substantially higher lifetimes under common contact loading conditions.

The issue of CTE stresses warrants additional consideration in the clinical context. When fusing porcelain to a core material, special attention is given to CTE matching. If the mismatch is too large it is impossible to prepare intact specimens. In our case the mismatch is within $2 \times 10^{-6} \text{ K}^{-1}$, not enough to cause failure during preparation, but, in the case of alumina, enough to negate the benefits of a high core modulus. As our comparative alumina and zirconia data verify, it is better to err such that the veneer has a slightly lower CTE than the core.⁷

The issue of joining also warrants further deliberation. Fusion processes, while subject to deleterious CTE stresses, produce relatively strong interfaces, lowering the risk of delamination and spallation. We have sought to circumvent the CTE issue in our experiments by using an epoxy adhesive at room temperature. However, such interfaces are relatively weak and therefore subject to delamination and spalling. Moreover, if the epoxy layer is too thick the flexure of the veneer is enhanced resulting in premature initiation of radial cracks at the veneer (rather than core) bottom surface.¹¹ Further investigation into alternative low-temperature joining methods using stronger and stiffer bonding agents could prove fruitful.

Our present study has focused on cone cracking in the veneer layer. We have alluded to other potentially dangerous failure modes. Arguably the most important of these is radial

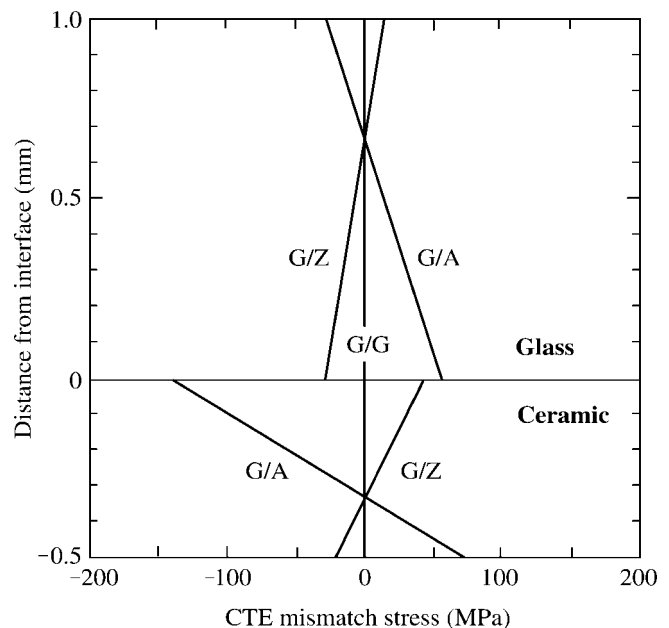


Figure 8. Distribution of residual CTE stresses in fused glass/alumina (G/A) and glass/zirconia (G/Z) bilayers relative to all-glass control (G/G), for bilayer with ideal interface and polycarbonate base.

cracking in the support core.^{6,12,15} Note the magnified stresses at the core bottom surface in Figure 7, reflecting a large component of layer flexure in the loading. The pervasive dominance of cone cracking is contingent on several factors. One factor is the net veneer/core thickness d . If d remains larger than about 1.5 mm or more, core radial cracking may effectively be suppressed in any material combination.¹⁵ However, the critical load to initiate core radials is proportional to d^2 , so any reduction in d can quickly tilt the balance toward radial crack failure. In addition, a stiff core supports more of the applied load, and hence concentrates stress more strongly at the bottom surface (Figure 7).¹⁶ Alumina is particularly vulnerable because of its combination of higher stiffness and lower strength.¹⁵ Moreover, as seen above, residual stresses can strongly exacerbate this vulnerability (Figure 8). For these reasons, zirconia might appear to be a better candidate as a core material in dental crowns. On the negative side, Y-TZP is thermodynamically unstable in moist environments, leading to progressive damage accumulation with age.¹⁷ Composite two-phase alumina–zirconia materials, which minimize any such instability and yet retain some of the beneficial mechanical properties of zirconia, may offer an attractive route to next-generation biomedical materials.¹⁸

Assistance with experimental data from Juan José Meléndez-Martínez is gratefully acknowledged. Information of product names and suppliers in this paper is not to imply endorsement by NIST.

REFERENCES

1. Frank FC, Lawn BR. On the theory of Hertzian fracture. *Proc R Soc London A* 1967;299:291–306.
2. Lawn BR. Indentation of ceramics with spheres: A century after Hertz. *J Am Ceram Soc* 1998;81:1977–1994.
3. Zhang Y, Bhowmick S, Lawn BR. Competing fracture modes in brittle materials subject to concentrated cyclic loading in liquid environments: Monoliths. *J Mater Res* 2005;20:2021–2029.
4. Bhowmick S, Zhang Y, Lawn BR. Competing fracture modes in brittle materials subject to concentrated cyclic loading in liquid environments: Bilayer structures. *J Mater Res* 2005;20:2792–2800.
5. Zhang Y, Kwang J-K, Lawn BR. Deep penetrating conical cracks in brittle layers from hydraulic cyclic contact. *J Biomed Mater Res B Appl Biomater* 2005;73:186–193.
6. Hermann I, Bhowmick S, Zhang Y, Lawn BR. Competing fracture modes in brittle materials subject to concentrated cyclic loading in liquid environments: Trilayer structures. *J Mater Res* 2006;21:512–521.
7. McLean JW. *The Science and Art of Dental Ceramics, Vol. 1: The Nature of Dental Ceramics and Their Clinical Use*. Chicago: Quintessence; 1979.
8. Lee KS, Jung Y-G, Peterson IM, Lawn BR, Kim DK, Lee SK. Model for cyclic fatigue of quasiplastic ceramics in contact with spheres. *J Am Ceram Soc* 2000;83:2255–2262.
9. Lawn BR, Deng Y, Miranda P, Pajares A, Chai H, Kim DK. Overview: Damage in brittle layer structures from concentrated loads. *J Mater Res* 2002;17:3019–3036.
10. Taskonak B, Mecholsky JJ, Anusavice KJ. Residual stresses in bilayer dental ceramics. *Biomaterials* 2005;26:3235–3241.
11. Chai H, Lawn BR. Role of adhesive interlayer in transverse fracture of brittle layer structures. *J Mater Res* 2000;15:1017–1024.
12. Chai H, Lawn BR, Wuttiphan S. Fracture modes in brittle coatings with large interlayer modulus mismatch. *J Mater Res* 1999;14:3805–3817.
13. Schwarzer N, Chudoba T, Pharr GM. On the evaluation of stress in coated materials during nanoindentation with sharp indenters. *Surf Coat Technol* 2006;200:4220–4226.
14. Jung YG, Wuttiphan S, Peterson IM, Lawn BR. Damage modes in dental layer structures. *J Dent Res* 1999;78:887–897.
15. Deng Y, Miranda P, Pajares A, Guiberteau F, Lawn BR. Fracture of ceramic/ceramic/polymer trilayers for biomechanical applications. *J Biomed Mater Res A* 2003;67:828–833.
16. Miranda P, Pajares A, Guiberteau F, Deng Y, Zhao H, Lawn BR. Designing damage-resistant brittle-coating structures. II. Trilayers. *Acta Mater* 2003;51:4357–4365.
17. Chevalier J. What future for zirconia as a biomaterial? *Biomaterials* 2006;27:535–543.
18. Willmann G. Improving bearing surfaces of artificial joints. *Adv Eng Mater* 2001;3:135–141.